J Mol Model (2006) 12: 885–896
DOI 10.1007/s00894-005-0053-3

ORIGINAL PAPER

Parawan Chuichay · Egor Vladimirov · Khatcharin Siriwong · Supot Hannongbua · Notker Rösch

Molecular-dynamics simulations of pyronine 6G and rhodamine 6G dimers in aqueous solution

Received: 5 September 2005 / Accepted: 21 September 2005 / Published online: 23 June 2006

Abstract We have carried out molecular-dynamics (MD) simulations on dimers of the positively charged laser dyes pyronine 6G (P6G) and rhodamine 6G (R6G) in aqueous solution, generating trajectories of 2.5 ns for various computational protocols. We discuss how the choice of atomic partial charges and the length of the trajectories affect the predicted structures of the dimers and compare our results to those of earlier MD-simulations, which were restricted to only 0.7 ns. Our results confirm that monomers of P6G easily undergo relative rotations within the dimer, but we found new conformations of the R6G dimer at longer simulation times. In addition, we analyzed in detail the energy change during the formation of dimers. With suitable corrections, the electrostatic energy from an Ewald treatment agrees with the results from an approach relying on a residue-based cutoff. For P6G, we show that the strong solvent-mediated electrostatic attraction between the monomers is counteracted by an almost equally large solvent-induced entropy contribution to yield a small driving force to dimer formation, in very good agreement with the free-energy change from a thermodynamic-integration procedure. Thus, earlier rationalizations of the dimer formation, based only on energy arguments, yield a qualitatively wrong picture.

Electronic Supplementary Material Supplementary material is available for this article at http://dx.doi.org/10.1007/s00894-005-0053-3 and is accessible for authorized users.

P. Chuichay · E. Vladimirov · K. Siriwong · N. Rösch (✉)
Department Chemie Technische Universität München,
85747 Garching, Germany
e-mail: roesch@ch.tum.de

P. Chuichay · S. Hannongbua
Computational Chemistry Unit Cell,
Faculty of Science, Chulalongkorn University,
Bangkok 10330, Thailand

K. Siriwong
Department of Chemistry,
Faculty of Science,
Khon Kaen University,
Khon Kaen 40002, Thailand

Keywords Rhodamine · Ion dimers · Free energy calculations · Molecular dynamics simulations

Introduction

Xanthene molecules are well known for their remarkable photophysical properties. Therefore, they are frequently used as efficient laser dyes and fluorescent probes attached to molecules of biological interest [1–6]. However, aggregation of these dye molecules in aqueous solution [3, 7] can interfere with their successful usage due to a drastic drop-off in the fluorescence quantum yield, discernible even at very low concentrations of ~10^{-6} M [8].

Self-aggregation of xanthene dyes poses a non-trivial physico-chemical problem because in general these molecules are positively charged, so that, at first glance, the interaction among such moieties is anticipated to be repulsive. Usually, aggregation in aqueous solution is observed for non-polar neutral molecules and ascribed to "hydrophobic interactions" [9], whereas recent molecular-dynamics simulations on picrate anions in water revealed a definite trend for these charged moieties to form aggregates up to tetramers [10]. Thus, the atomistic mechanism of the latter type of aggregation has remained controversial.

Association between ions of like charge could be caused by a number of possible physical mechanisms, ranging from direct bonding to simultaneous attachment to a third species. A special case of these interactions might be represented by π-stacking between flat, like-charged aromatic moieties [11]. The molecular mechanism of π-stacking, although directly observed in many organic and bioorganic systems, has not yet been fully rationalized theoretically, even for the case of neutral species [12–14]. Indeed, systematic theoretical studies on the π-stacking of like-charged aromatic residues are still rare [7, 10].

Hence, self-aggregation of xanthene-dye molecules represents an interesting challenge for theoretical studies. Recently, Daré-Doyen et al. presented a molecular-dynamics (MD) study on pyronine 6G (P6G) and rhodamine 6G (R6G) dimers in aqueous solution [7]. However, these MD-

simulations comprised rather short trajectories and some uncertainties remained regarding the force-field description. In particular, the atomic (partial) charges on the dye molecules do not seem to have been chosen according to standard procedures consistent with the force field used.

These issues needed to be clarified before we were able to tackle MD-simulations on the structure and relative mobility of rhodamine–DNA complexes, currently under study [15]. Therefore, we undertook a more detailed computational study to establish a suitable protocol for MD-simulations of dimers of P6G and R6G (Fig. 1) in aqueous solution. In the following, we will present and discuss these results and compare them to those of previous investigations [7].

Materials and methods

We carried out MD-simulations using the program suite AMBER 8 [16]. For continuity with previous MD-simulations on DNA duplexes, [17, 18] we chose the force field AMBER-95 [19]. This and also a more recent variant of the AMBER force field [20] require that partial atomic charges be supplemented when used for the chromophores under study. The recommended procedure for generating atomic charges for AMBER 8 is based on a point-charge representation of the electrostatic potential (ESP) as obtained from an HF-SCF calculation with a 6–31G* basis set [19]. Strong local "variations" among atomic charges are controlled with a penalty function, applied in the "restrained" version (RESP) [21] of the Merz–Kollman ESP-fitting procedure [22, 23]. Unless mentioned otherwise, we based the determination of atomic charges on molecular geometries optimized at the B3LYP/6–31G* level.

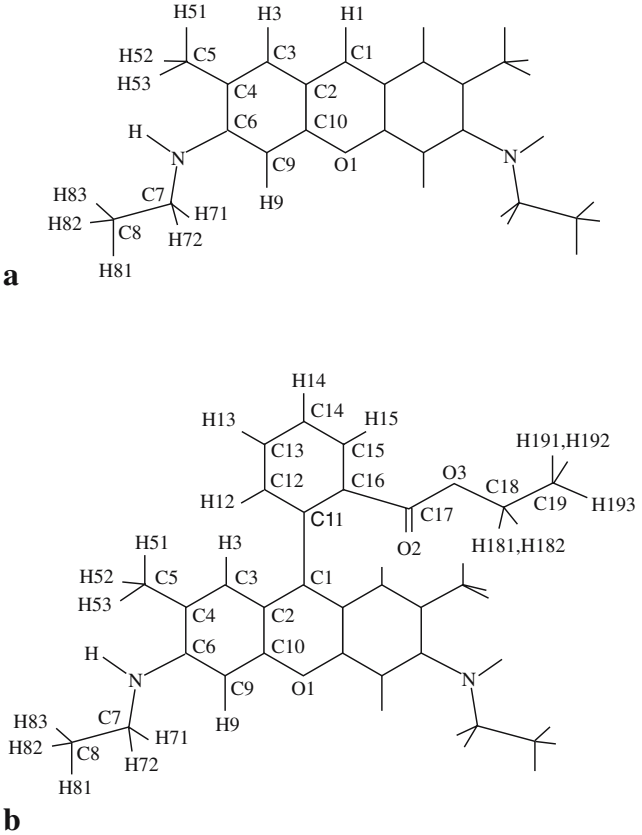

Fig. 1 Structure and atom labels for **a** pyronine 6G (P6G) and **b** rhodamine 6G (R6G)

All electronic structure calculations were carried out with the program package Gaussian98 [24]. However, we were unable to reproduce the charge values suggested by Daré-Doyen et al. (in the following designated "DD") [7] when we checked the RESP atomic charges for both P6G and R6G, using an HF/6–31G* description (in the following referred to as "STD"), which is the recommended standard for supplementing the force field AMBER-95 [16, 25] see Table 1.

To clarify this discrepancy, we explored RESP atomic charges for P6G and R6G in more detail. First, we compared charge results for P6G from HF-SCF calculations with basis sets of increasing flexibility, namely 6–31G, 6–31G*, 6–31G**, and 6–311G** (Table S1 of the Electronic Supplementary Material, ESM). On going from the 6–31G to the 6–31G* (STD) basis set, i.e. by including polarization functions on non-hydrogen centers, the average absolute charges change by 0.03 *e*. By far the largest changes occur at the oxygen center O1 and its carbon neighbors C10; both charges decrease (by absolute value), i.e. for O1 from −0.439 *e* to −0.282 *e* and for C10 from 0.568 *e* to 0.426 *e*. Inclusion of polarization functions for hydrogen atoms (6–31G**) does not alter the charge distribution noticeably compared to the STD results, with an average absolute change of 0.004 *e*; the largest variation of an atomic charge was found for the carbon centers C7 within the ethyl substituents of the nitrogen centers, namely 0.040 *e* and 0.028 *e* for 6–31G* and 6–31G**, respectively. Atomic partial charges vary somewhat more when the basis set is increased to triple-ζ quality, 6–311G**; the average absolute change was 0.010 *e*. We also determined RESP charges from a charge distribution generated at the B3LYP/6–31G* level; these charges are, in general, smaller by absolute value, i.e. the charge distribution appears to be locally less polarized than in the STD case (Table S1). Finally, we also studied charges for a geometry determined at the HF/6–31G level as indicated by Daré-Doyen et al. [7] but the RESP charges are hardly affected if derived from charge distributions of the same level, B3LYP/6–31G* or HF/6–31G. At the electronic structure level used by Daré-Doyen et al. [7], HF/6–31G for both structure and charge distribution, we also probed the differences between the RESP scheme [21] and the original ESP variant [22, 23] as well as another version of potential-derived charges [26] (Table S1). However, with all these variations of the computational procedure, we were unable to reproduce the DD charges of [7].

As the STD and DD solutions of the reverse problem of electrostatics differed significantly, we decided also to study the resulting electrostatic model potentials V_{STD} and

Table 1 RESP charges of pyronine 6G and rhodamine 6G molecules[a]

	Pyronine 6G		Rhodamine 6G	
	DD	STD	DD	STD
C1	0.256	0.048	0.363	0.135
C2	−0.318	−0.118	−0.303	−0.104
C3	−0.211	−0.246	−0.237	−0.270
H3	0.218	0.206	0.213	0.213
C4	0.081	0.072	0.096	0.083
C5	−0.454	−0.286	−0.397	−0.299
H51–H53	0.152	0.101	0.129	0.101
C6	0.522	0.269	0.410	0.261
N	−0.742	−0.412	−0.608	−0.423
H	0.414	0.329	0.375	0.327
C7	0.382	0.040	0.271	0.062
H71–H72	−0.001	0.097	0.029	0.090
C8	−0.304	−0.315	−0.335	−0.319
H81–H83	0.086	0.107	0.099	0.105
C9	−0.680	−0.436	−0.550	−0.442
H9	0.251	0.182	0.205	0.181
C10	0.627	0.426	0.524	0.428
O1	−0.390	−0.282	−0.328	−0.287
H1/C11	0.135	0.170	0.204	0.123
C12	–	–	−0.284	−0.194
H12	–	–	0.172	0.154
C13	–	–	−0.051	−0.114
H13	–	–	0.165	0.169
C14	–	–	−0.180	−0.115
H14	–	–	0.172	0.159
C15	–	–	−0.109	−0.146
H15	–	–	0.190	0.174
C16	–	–	−0.223	−0.161
C17	–	–	0.838	0.822
O2	–	–	−0.538	−0.568
O3	–	–	−0.561	−0.489
C18	–	–	0.381	0.383
H181–H182	–	–	0.005	−0.003
C19	–	–	−0.253	−0.293
H191–H193	–	–	0.070	0.087

[a]From a single-point HF/6–31G* calculation on the B3LYP/6–31G* geometry. For the designation of the atoms, see Fig. 1

V_{DD} via their relative difference $R(r) = \Delta V(\mathbf{r})/\overline{V}(\mathbf{r}) = 2(V_{DD} - V_{STD})/(V_{DD} + V_{STD})$ We checked R for P6G in planes parallel to the molecular plane and found that its maximum value decreased from 6–7% in the plane at a distance of 3.5 Å from the molecular plane to 3–4% in the plane at 5.5 Å. As another direct comparison, we mention electrostatic potential energy curves during the relative rotation of the monomers in P6G dimers. That interaction features a double minimum shape, again with small but distinct differences (Fig. S1; see ESM). At an inter-planar separation of 3.8 Å, the two minima are located at torsion angles β (see below) of ~90° and ~270°, but these angles differ by about 10° between the two sets of charges. Also the barriers at 0° twist, ~5 kcal mol^{-1}, differ by ~10%. Although these differences between the two representations of the electrostatic interaction may seem small, they can affect the dynamics of the dimers at longer times significantly. We note in passing that the minima of the electrostatic interaction at twist angles of ~90° and ~270° indicate a dominant role of the quadrupole over the dipole term; of course, at such short inter-planar distances, an argument based on dipole and quadrupole terms cannot be quantitative.

In a further step of our "sensitivity analysis" of the force field used, we probed the different treatments of the electrostatic interaction. As a standard, we used the particle-mesh Ewald (PME) technique [27, 28] with the default parameters as implemented in AMBER 8 [16, 25]. Daré-Doyen et al. [7], after some test calculations, had opted for the residue-based cutoff procedure implemented in older versions of AMBER. Thereby, if any pair of atoms of two "residues" (molecular moieties) was inside the cutoff, the nonbonding and electrostatic interactions between *all* atom pairs of these two residues were included. From version 6 on, AMBER switched to an atom-based interpretation of

the cutoff and a PME treatment of the electrostatic interactions as standard [29].

In view of these methodological issues, we carried out MD-calculations for P6G and its dimers, for both STD and DD charges, to study structural and dynamic effects of these force-field parameters in a consistent fashion. We checked the consequences.

Furthermore, for each of these two force field variants, we generated MD-trajectories with and without invoking the PME technique. In calculations with Ewald summation, we applied a cutoff of 10 Å to the van der Waals interactions, but like Daré-Doyen et al. [7] we used an overall cutoff of 12 Å (non-bonding and Coulomb interactions) in calculations that invoked a residue-based selection of the electrostatic interaction. In this way, the electrostatic interaction between the two monomers of a xanthene dimer was always accounted in full. These latter calculations were carried out with the module Sander_Classic of AMBER 6 [25].

All MD-simulations were performed for dye molecules in aqueous solution. For this purpose, we inserted each system into a rectangular box containing TIP3P water molecules [30] and applied periodic boundary conditions. Table S2 of the ESM shows the dimensions of the boxes and the numbers of water molecules for the various solutes. To compensate the positive charge of each chromophore and to render the whole system neutral, we added a chloride ion per dye molecule to each box.

We followed the usual procedures to establish initial structures of MD runs. We first obtained equilibrium geometries [16, 25, 31, 32] and then we generated the dynamics, invoking the SHAKE algorithm for bonds involving H atoms [33, 34]. Specifically, we started each simulation with a minimization of the total energy by applying a conjugate gradient optimization to the solvent structure. Then we carried out a series of equilibration MD runs on the water structure at pressure P=1 atm while we kept the structure of the solute fixed. Over 20 ps, the system was gradually heated to 300 K and then was maintained at that temperature for 80 ps; here, as in all MD runs, the time steps were 2 fs. Afterwards, MD-production runs were performed for at least 2.5 ns using an NPT ensemble with temperature T=298 K and pressure P=1 atm. For each system under study, we analyzed the MD trajectories in two time ranges, based on structure snapshots taken at each picosecond. To compare with the simulations of Daré-Doyen et al. [7], we treated the first 700 ps of a production trajectory separately. Then, we extended the MD trajectory by 800 ps without analysis. Finally, we analyzed the MD trajectory from 1.5 to 2.5 ns.

We used four variables to quantify the structure of a dimer. The definition of these parameters starts with two pertinent characteristics, namely the average plane P of each xanthylium group and its center of mass M. (The xanthylium group comprises the set of 14 atoms which make up the three aromatic rings; Fig. 1). Then four key structure parameters of a dimer are (1) the distance M–M between the two centers of mass M and M′ of each xanthylium group, (2) the average M–P of the two distance M–P′ and M′–P between the center of mass M of one xanthylium system to the plane P′ of the second xanthylium system of a dimer and vice versa, and (3) the roll angle α between the two xanthylium planes P and P′, and (4) the torsion angle β, i.e. the dihedral angle C1–M–M′–C1′ (see Figs. 1 and 2). Daré-Doyen et al. used a different dihedral angle, C1–M–C1′–M′ which they also called β; [7] to avoid confusion, we refer to that dihedral angle as β'. The anti-parallel reference configuration of a dimer is characterized by β=180° and β'=0°. For the dominant range of inter-plane distances, the torsion angles β and β' essentially complement each other to 180° within a few degrees.

We started the MD-simulations of P6G dimers with the monomers (in the geometry optimized at the B3LYP/6–31G* level) oriented in anti-parallel fashion (Fig. 2), eclipsed at an inter-plane separation of 3.8 Å. For the R6G dimer, we used two starting geometries (Fig. 3): (1) an anti-parallel configuration (β=180°) in full analogy to the P6G dimer, and (2) a "twisted" configuration with β=120° at an inter-plane separation of 6 Å. In addition, we carried out a simulation of the R6G dimer where the monomers were initially separated by 10 Å with β=180°.

To obtain the free-energy profile for the interaction of two P6G units at varying distance, we invoked thermodynamic integration [35]. For this purpose, we resorted to the module GIBBS of AMBER 6 [25]. We defined holonomic distance constraints [36] via the non-interacting centroids of the two monomers (Fig. S2; see ESM). That constrained distance was changed in steps of 0.25 Å from 2.5 to 4.0 Å and then in steps of 0.5 Å up to a maximum of 12 Å. In

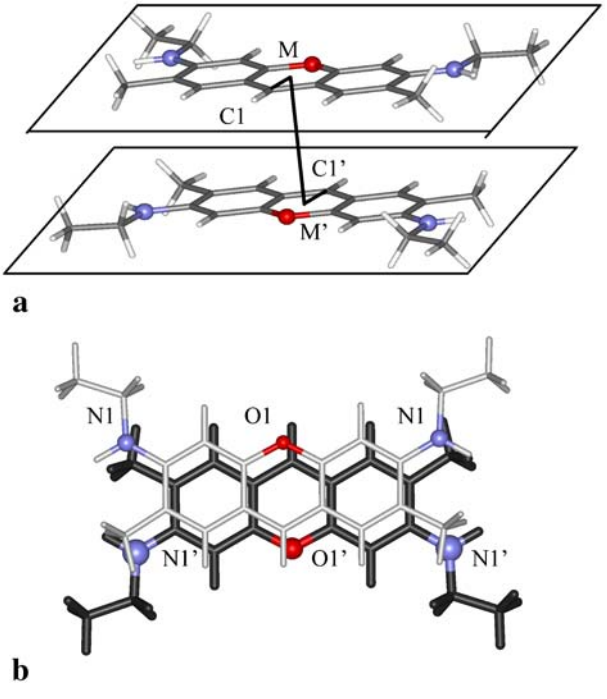

Fig. 2 **a** Torsion angle β=C1–M–M′–C1′ and M–M distance M–M', defined for the P6G dimer: M is the center of mass of the 14 heavy atoms in xanthylium rings. **b** P6G dimer in which monomer1 (*light and thin*) is above monomer2 (*dark and thick*) in antiparallel configuration, β=180°

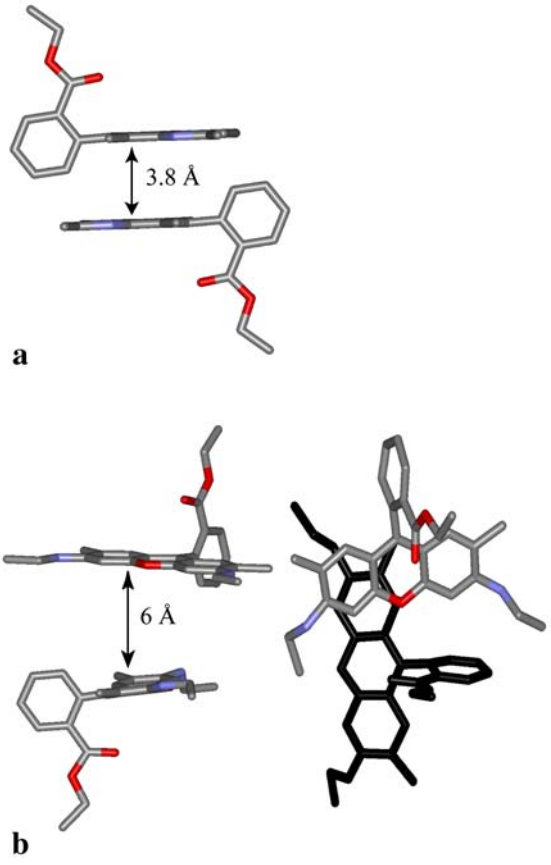

Fig. 3 Starting geometries of the two trajectories of R6G dimers: **a** antiparallel orientation, β=180°; **b** twisted configuration with β=120°

each of the 24 cases, after an equilibration phase of 20 ps, the data was collected for 180 ps at each ps. These simulations were carried out under the same conditions applied previously (NPT ensemble, PME treatment of electrostatic interactions), except time steps of 1 fs were used. Solute and solvent were separately coupled to a heat bath with the Berendsen algorithm [37].

Results and discussion

Structure and dynamics of pyronine dimers

We begin our discussion of the MD-results by analyzing structure and dynamics of a P6G dimer because the carbethoxyphenyl substituent of R6G complicates matters for such a dimer, Fig. 1. Table 2 summarizes the main structural findings from our MD simulations. Starting with the most accurate results, obtained by averaging data generated with the PME approach for the "long time" interval from 1.5 to 2.5 ns, we note that the M–M distances for the force field variants STD, (4.25±0.53) Å, and DD, (4.16±0.54) Å, are compatible. As expected for geometric reasons, the corresponding average M–P distances are shorter, (3.44±0.21) and (3.46±0.21) Å, respectively (Table 2). These latter distances between the planes of π-stacks are quite comparable to literature data [12–14]. The xanthylium planes stay parallel to each other, with an average roll angle α of (11±7)° for STD and (10±7)° for DD parameters. Also the torsion angles β, (55±33)° for STD and (56±34)° for DD, compare well for both variants of the force field (Table 2). The torsion angles β vary over a rather wide range, with standard deviations (SD) of ~30°, but the average configuration is closer to a parallel arrangement of the xanthylium groups than to an anti-parallel configuration (see below). As expected, the alternative torsion angle β' is essentially the complement of β to 180°. At long times, both force field variants, STD and DD, yield essentially the same standard deviations for each of these structure parameters.

Table 2 Geometric parameters[a] of a pyronine 6G dimer, averaged over various time intervals of MD trajectories. Results are shown for various force field variants (STD, DD) and two treatments of the electrostatic interaction, particle mesh Ewald technique (PME) and a residue-based cutoff of 12 Å

Charges		1–700 ps			1,501–2,500 ps	
		STD[b]	DD[c]	DD/PW[d]	STD[b]	DD[c]
M–M, Å	PME	4.08±0.52	4.17±0.59	–	4.25±0.53	4.16±0.54
	Cutoff	4.21±0.58	4.36±0.47	4.14±0.52	4.24±0.43	4.19±0.57
M–P, Å	PME	3.40±0.20	3.50±0.21	–	3.44±0.21	3.46±0.21
	Cutoff	3.45±0.25	3.54±0.20	3.43±0.25	3.48±0.16	3.46±0.20
Roll α, °	PME	12±8	10±9	–	11±7	10±7
	Cutoff	12±10	12±10	9±18	9±5	9±6
Torsion β, °	PME	95±40	109±57	–	55±33	56±34
	Cutoff	141±37	161±16	–	37±19	47±26
Torsion β', °	PME	89±36	70±56	–	124±30	123±31
	Cutoff	41±37	19±17	4±18	139±19	130±26

[a]See Fig. 2 for the definitions
[b]Standard force field, present work
[c]Atomic partial charge from [7], present work
[d]Previous work, [7]

Next, we compare the results of Table 2 according to three criteria that reflect on alternative MD strategies [7]. First, we address the effect of using a residue-based cutoff of 12 Å for the Coulomb interaction, based on the more accurate long-time averages (1.5–2.5 ns). For each set of charges, STD and DD, the long-time average values of all four structural parameters, M–M, M–P, α, and β, from the trajectory obtained with Coulomb cutoff are compatible with the corresponding averages obtained with the PME treatment (Table 2). For both STD and DD results, there is a trend to smaller SD values of all characteristics shown in Table 2 (with the exception of M–M for DD charges), on going from PME results to those obtained with a Coulomb cutoff. Still, according to these long-time results, we can confirm the conclusion [7] that for the present systems the PME method and the residue-based cutoff of the Coulomb interaction yield results that are comparable to a large degree.

This brings us to our second comparison, namely long-time (1,501–2,500 ps) vs. short-time (1–700 ps) trajectory averages (Table 2). The corresponding averages and standard deviations of the distances M–M and M–P as well as of the roll angle α are essentially compatible between all MD set-ups (STD vs. DD, PME vs. cutoff). However, long-time and short-time results for the torsion angle β (and its complement β') are noticeably different.

At short times, PME results for both variants of the force field, STD and DD, exhibit a propensity to larger values of the torsion angle β (Fig. 4), (95±40)° vs. (55±33)° and (109±57)° vs. (56±34)°, respectively. In particular, the SD values are significantly larger at shorter times (PME: 40°, 57° vs. 33°, 34°; Table 2). In fact, as these MD trajectories had been started in the anti-parallel configuration, β=180°, following the suggestion of earlier work [7], they took some time to reach smaller torsion angles. This effect is particularly noticeable for trajectories generated with Coulomb cutoff, where large values of β dominate for the first 500–600 ps (Fig. 4). This analysis confirms that short simulation times of at most 700 ps, as adopted in [7], are not adequate for sampling the phase space. The subsequent discussion of physical aspects will be based only on structural parameters averaged over later times, from 1.5 to 2.5 ns.

Based on the long-time averages, we turn to the differences caused by the force-field variants STD and DD as third aspect of the comparison. Above we noted some differences in the structural parameters between the two sets of partial atomic charges when a Coulomb cutoff was employed (Table 2). However, with the PME approach, the two sets of charges yield very similar results. Still, the STD charges are preferable for consistency with the AMBER protocol of charge assignment [19].

Summarizing our methodological study, we decided to base our interpretation of *physical* properties of xanthene dimers in aqueous solution on MD simulations (1) obtained with the RESP-based charge assignment STD, (2) employing the PME technique for an accurate representation of the Coulomb interactions, and (3) using only data from later sections of trajectories, beyond 1 ns (Figs. 4 and 5). In contrast, the previously suggested physical picture, results DD/PW of Table 2, [7] were gleaned from a short trajectory

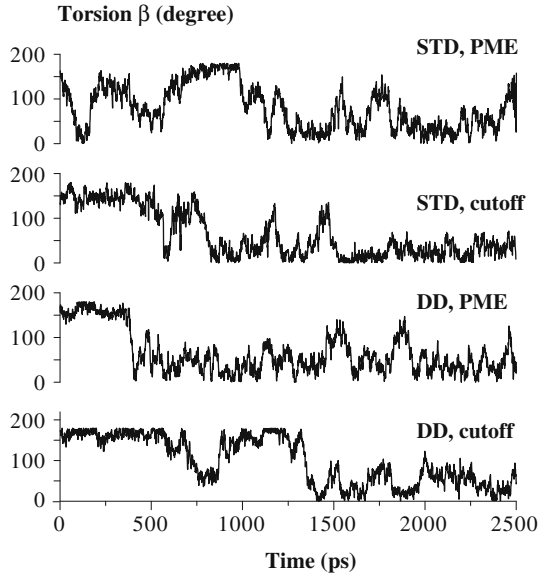

Fig. 4 Torsion angle β (see Fig. 2) of P6G dimers based on various MD protocols. Simulations treating the Coulomb interaction with a PME technique and a residue-based cutoff of 12 Å, for force-field variants with standard (STD) or DD charge assignment (see text)

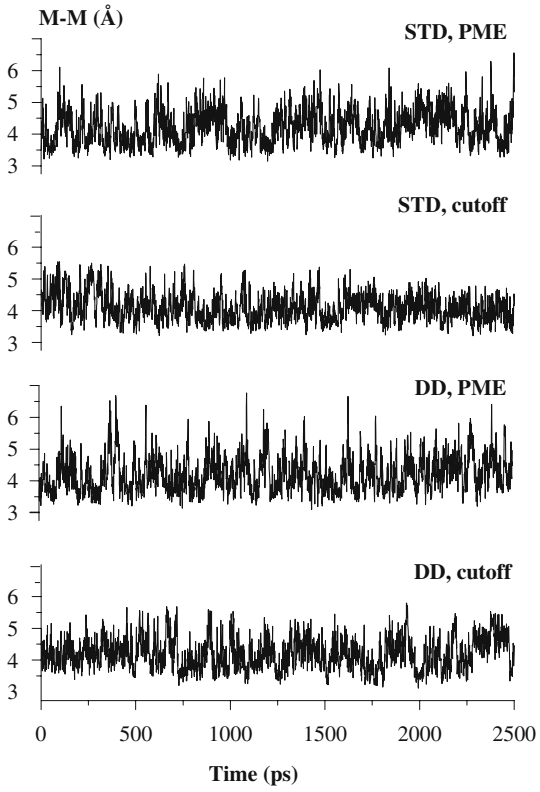

Fig. 5 M–M distance (see Fig. 2) in pyronine 6G dimers based on various MD protocols. Simulations treating the Coulomb interaction with a PME technique and a residue-based cutoff of 12 Å, for force-field variants with standard (STD) or DD charge assignment (see text)

(up to 700 ps), generated with a Coulomb cutoff. Based on the pertinent structural parameters of Table 2, our present results suggest a very similar picture for P6G dimers than discussed previously [7]—with one notable exception. DD/PW results [7] and long-time STD/PME averages of the present work for the torsion angle β' do not agree at all (Table 2). Whereas previously an anti-parallel orientation of the two monomers was found, β'=(4±18)°, our best results indicate rather large values for the alternative torsion angle, β'=(124±30)°, which in addition fluctuates over a wider range.

Structure and dynamics of rhodamine 6G dimers

Now we turn to the simulations of R6G dimers in aqueous solution, which were obtained with STD charges and the PME method. To facilitate comparison with previous work [7] we again considered two parts of a 2.5 ns trajectory, separately averaging over a short-time window, up to 0.7 ns, and a long-time window, from 1.5 to 2.5 ns (Table 3). We will first discuss the results for the trajectory which, as done before, [7] was started with an anti-parallel orientation, β=180°, of the xanthylium moieties. For the short-time window, results for the key structure parameters M–M (Fig. 6a), M–P, roll angle α, and twist angle β indeed agree well with previous results [7] and with the results obtained for a P6G dimer (Table 2). For the long-time average, one notes a propensity to larger M–M distances, (4.41±0.50) Å compared to (3.83±0.26) Å at shorter times, and shorter M–P distances, (3.34±0.25) Å compared to (3.62±0.16) Å at shorter times. Yet, corresponding averages at different times are compatible, based on the SD values.

However, this correspondence of short-time and long-time averages does not extend to the torsion angle β (Table 3). After 1.5 ns, the R6G dimer exhibits a trend toward a twisted conformation at smaller torsion angles (Fig. 3b), with β=(135±19)° compared to the short-time average of (157±9)°. From the SD values, both averages are statistically compatible. To study this conformation effect in more detail, we started a second trajectory at β=120° (see Section Materials and Methods). After some structural adjustment, the torsion angle of this new trajectory settles near 70°, both for the short-time and the long-time average, with small and stable SD values of ~10° (Table 3). The smaller SD values for the averages of M–M and M–P of the second trajectory, 0.21 and 0.17 Å, respectively, compared to 0.50 Å and 0.25 Å (Table 3), indicate that this "twisted" configuration is more stable than the "anti-parallel"

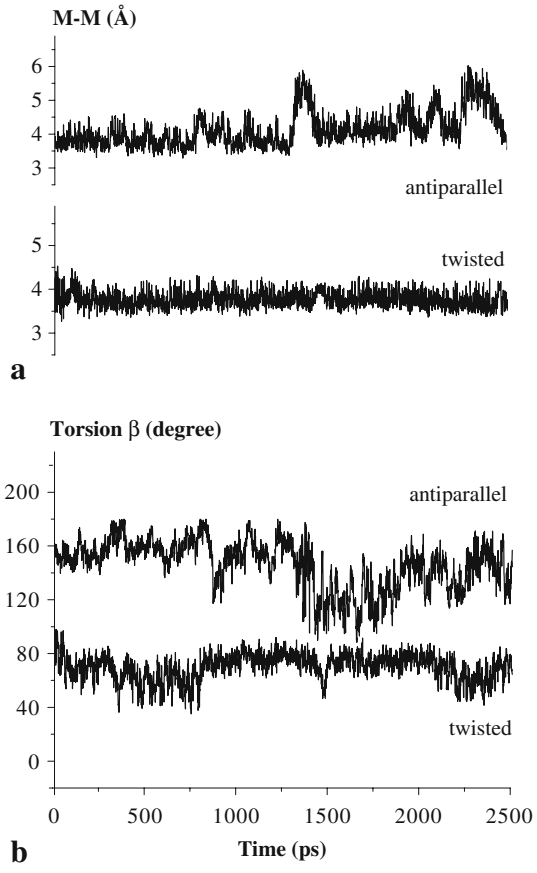

Fig. 6 M–M distance (**a**) and torsion angle β (**b**) of R6G dimers from MD set-ups with anti-parallel and twisted (β=120°) initial configurations; see Fig. 3. Simulation based on the STD charge assignment, treating the Coulomb interaction with the PME technique

Table 3 Geometric parameters[a] of a rhodamine 6G dimer, averaged over various time intervals of MD trajectories with different initial structures (β=120°, 180°). Results for the STD variant of the force field and the PME treatment of the Coulomb interactions. Also shown are results of a previous study (DD/PW)

	1–700 ps			1,501–2,500 ps	
Charges	STD[b]	STD[b]	DD/PW[c]	STD[b]	STD[b]
Initial structure	β=120°	β=180°	β=180°	β=120°	β=180°
M–M, (Å)	3.91±0.62	3.83±0.26	3.75±0.23	3.77±0.21	4.41±0.50
M–P, (Å)	3.61±0.25	3.62±0.16	3.47±0.32	3.58±0.17	3.34±0.25
Roll α, °	23±6	8±6	10±6	23±5	15±9
Torsion β, °	66±12	157±9	–	71±10	135±19
Torsion β, °	117±12	25±10	20±11	111±11	56±20

[a]See text and Fig. 2 for the definitions
[b]Standard force field, present work
[c]Previous work, [7]

configuration reached at long times on the trajectory started with β=180°.

The results for the second trajectory clearly identify a different conformation that is statistically independent from the conformation of the trajectory started with an anti-parallel orientation of the xanthylium rings (Fig. 6b). It seems that the long-time average of the torsion angle β (let alone the short-time average) correlates to some extent with the initial value of the trajectory. Therefore, trajectories even longer than 2.5 ns seem to be required to approach a representative sampling of phase space.

As for the P6G dimer, the results for the torsion angle disagree with those obtained previously [7]. The long-time average values of the alternative torsion angle β', (56±20)° for the trajectory starting at β=180° and (111±11)° for the trajectory starting at β=120°, describe rather different configurations of R6G dimers than previous results, β'=(20±11)° (Table 3). Therefore, torsion angles of the xanthene dimers seem to be the structure parameter most sensitive to parameters of the MD simulations, in particular to length of the MD trajectories.

The physical mechanism of dimer formation in aqueous solution

Finally, we turn to an exploration of the driving force responsible for the formation of dimers from two positively charged xanthene monomers. This issue deserves further study despite previous discussions [7, 10]. As a convincing demonstration of the strength of the driving force, we show in Fig. 7 results of an MD simulation on an R6G dimer where the trajectory was started with the two monomers separated by 10 Å. Within 150–200 ps, both characteristic distances M–M and M–P quickly reduce to their typical range of 4–5 and 3–4 Å, respectively, and a solvated dimer of two positively charged R6G monomers is formed.

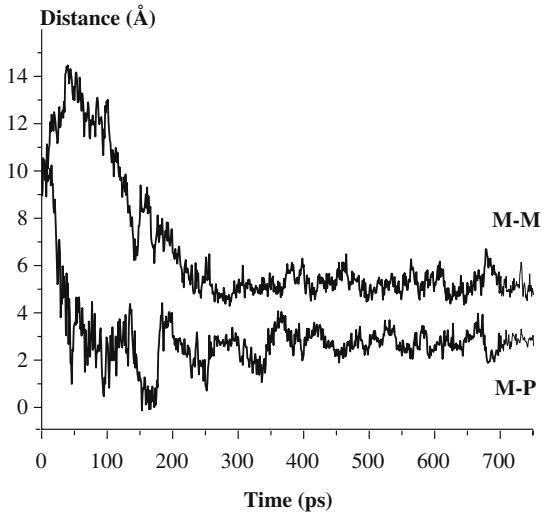

Fig. 7 Evolution of the M–M and M–P distances of a R6G dimer from an MD run starting in an anti-parallel configuration at an inter-plane separation of 10 Å. Simulation based on the STD charge assignment, treating the Coulomb interaction with the PME technique

It is informative, but as we will show not sufficient, to analyze the energy change underlying the dimer formation, based on those trajectories used previously to discuss the structure of the dimers (Table 4). For the present purpose, we separated, both for P6G and R6G dimers, the intra-dimer interactions (dye–dye) from the interaction of a dimer with its aqueous environment (dye–solv, Table 4), partitioning these interaction energies further into van der Waals (vdW) and electrostatic (estat) contributions. As reference, we also analyzed the interaction of dye monomers with their solvent, based on separate MD trajectories. With methodological issues in mind (see Section Structure and Dynamics of Pyronine Dimens), we compare in Table 4 results for the P6G dimer from trajectories with a cutoff-based and a PME treatment of Coulomb interactions (see Section Materials and Methods). We complement the analysis of a P6G monomer with results from a trajectory generated with a full Ewald treatment (Table 4).

Detailed inspection of the P6G data of Table 4 reveals three noteworthy results. (1) The intra-dimer interaction (dye–dye) is repulsive as electrostatic repulsion substantially exceeds van der Waals attraction, to yield a total repulsive energy of 31 kcal mol^{-1}. Therefore, dimerization cannot be discussed without accounting for effects of the solvent environment [7, 10]. (2) Including the solvent contributions, the total energy ΔE_{dim} of dimerization is very large, (−77±22) for the PME trajectory and (−56±36) kcal mol^{-1} for the cutoff-based trajectory. (3) This "reaction energy" is totally dominated by changes of the electrostatic interaction during dimer formation. The total van der Waals energy of a P6G dimer, intra-dimer plus dye-solvent interactions, is essentially the same as the van der Waals interaction of two monomers with their environment; the corresponding SD values are notably larger, 6–7 kcal mol^{-1}, than the net energy changes, −0.7 kcal mol^{-1} (cutoff) to −3.2 kcal mol^{-1} (PME) (Table 4).

We also would like to point out three method-oriented findings (Table 4). (1) Corresponding results on van der Waals energies from both trajectories, PME and cutoff-based, agree very well. (2) The same holds for the intra-dye interaction energies, including their van der Waals and electrostatic components. (3) In contrast, PME and cutoff-based results for the dye–solvent interactions, for both dimers and monomers, exhibit notable discrepancies. As typical result, we mention the electrostatic contribution to the interaction of a P6G dimer with the solvent, which is (−160±9) kcal mol^{-1} from the PME-based trajectory, but (−263±24) kcal mol^{-1} from the cutoff-based trajectory. Besides the large difference of the average values, one should also notice the much smaller SD value of the PME result. We obtained these results by following the standard procedure for evaluating electrostatic interactions with the AMBER package [16].

The PME results seemingly underestimate the solvation energies of monomers and dimers in a major way compared with the corresponding cutoff-based results. However, for a complete analysis of the electrostatic (free) energy of

Table 4 Energy component analysis[a] of monomers and dimers of P6G and R6G, based on trajectories up to 2.5 ns, generated with the standard variant (STD) of the force field and different treatments of the electrostatic interactions (PME, Ewald, cutoff)

		Dimer			Monomer		
		Dye–dye	Dye–solv	SE	Dye–solv	SE	ΔE_{dim}
P6G							
vdW	Ewald	–	–		−28.2±2.5		–
	PME	−14.0±1.5	−51.0±3.3		−30.9±2.5		−3.2±7.3
	Cutoff	−14.1±1.6	−49.0±3.2		−31.2±2.3		−0.7±7.1
estat	Ewald	–	–		−46.0±11.7		–
	PME	45.1±1.5	−159.6±9.2	−110.7±0.2	−47.1±4.9	−28.5±0.1	−74.0±15.9
	Cutoff	45.4±1.9	−262.9±23.8		−81.3±10.4		−54.9±36.1
Total	Ewald	–	–		−102.7±11.9		–
	PME	31.1±1.5	−321.3±12.7		−106.5±7.5		−77.2±21.7
	Cutoff	31.3±1.6	−311.9±23.6		−112.5±10.5		−55.6±35.7
R6G							
vdW	PME	−18.7±2.2	−66.2±4.4		−42.3±2.9		−0.3±9.5
estat	PME	42.1±1.7	−159.4±9.7	−98.6±0.1	−50.1±5.6	−26.5±0.2	−62.7±17.3
Total	PME	23.4±1.6	−324.2±10.0		−118.9±6.0		−63.0±17.6

[a]van der Waals (*vdW*), electrostatic (*estat*) and total contributions to the interaction between the two dye moieties of a dimer (dye–dye) as well as a between a solute (dimer, monomer) and its solvent environment (dye–solv). For PME trajectories, the self-energy correction (SE) is also given; see text for details. Binding energy of a dimer: $\Delta E_{dim} = E_{dimer}(dye-dye) + E_{dimer}(dye-solv) + (SE) - 2 \times [E_{monomer}(dye-solv) + E_{monomer}(SE)]$. All energies in kcal mol^{-1}

solvation based on an Ewald procedure, one has to add an estimate of the self-energy E_{SE}, which accounts for the interaction of a charge with its own periodic images and the neutralizing plasma [38]. For a cubic unit cell of length L (in Å), the self-energy term is $E_{SE} = -943.0\ q^2/L$ kcal mol^{-1} where q is the charge of the solvated molecule (in e) [39]. In the present study, the shapes of the unit cells are close to cubic; therefore, we estimated the self-energy correction by averaging $L^{-1} \approx V^{1/3}$ along a trajectory where V is the volume of the unit cell (Table S2). Other corrections, e.g. for a solvent of low dielectric permittivity [40] or the formation of a solute cavity of non-negligible size (radius R) compared to the unit cell [41], can be neglected in the present case because $1 << \varepsilon$ and $2\pi R^2/3L^2 << 1$, respectively. With the resulting E_{SE} corrections, PME and cutoff-based electrostatic energy contributions for monomers and dimers of both P6G and R6G agree within their standard deviations (Table 4).

We close this discussion of Table 4 by comparing results for P6G and R6G. Not unexpectedly, all van der Waals contributions of P6G, intra-dimer and dimer-solvent of the dimer and monomer-solvent, are larger (by absolute value) than the corresponding values for the smaller molecule P6G. However, just as for P6G, the van der Waals interaction of R6G does not provide a net contribution to the dimer formation, (−0.3±9.5) kcal mol^{-1}. Again as a consequence of the size of the systems, the electrostatic and the total interaction within a dimer are less repulsive for R6G, e.g. (23.4±1.6) kcal mol^{-1} for the total energy contribution compared to (31.1±1.5) kcal mol^{-1} for P6G. Also for R6G, the self-interaction corrected electrostatic interaction completely dominates the total energy of dimer formation, (−63.0±17.6) kcal mol^{-1}. Although this average value for R6G is notably smaller than the corresponding PME result for P6G, (−77±22) kcal mol^{-1}, one cannot draw any conclusions (e.g. on the equilibrium constants in solution), because both values are compatible within the sum of their standard deviations, ~30 kcal mol^{-1}.

This analysis of interaction energies yielded dimerization energies comparable to the solvation free energies of ions. Therefore, any direct comparison with experiment based on such an energy analysis [7] is premature without accounting for entropy contributions due to the reorganization of the solvent structure. Entropic effects due to the solute can be largely neglected because structure and internal energy of the xanthylium unit are not expected to undergo substantial changes during dimer formation; freezing the "flipping" degrees of freedom of the carbethoxyphenyl moieties would only lead to the loss of a few kcal mol^{-1}.

In simulations, solute-solvent entropy effects can directly be addressed based on solute-solvent distribution functions [42, 43]. Nevertheless, for a qualitative understanding of these effects as well as for assessing their scaling behavior with the charge and the size of the solute, it is useful to perform some very simplified estimates. One expects that the large favorable changes of the electrostatic energy upon dimerization are balanced by an decrease of the entropy due to a rearrangement of the water molecules in the vicinity of the solute. We estimate for P6G how the number of "bound" water molecules changes during the formation of a dimer.

As above, we focus on heavy atoms and we assume that each such center of a monomer is able to coordinate on average about two solvent molecules if no further steric constraints are active. Then a monomer is estimated to bind $N_{tot}(mono) = 2N$ water molecules, where N=22 for P6G. The value of $N_{tot}(mono)$=44 is in good agreement with the

number of water molecules in the first solvation shell of P6G, estimated along the trajectory by the program AMBER 8 on geometric grounds, [16] 45.1±3.8.

Upon formation of a dimer, the number of immobilized solvent molecules changes for both steric and electrostatic reasons. Extending the preceding steric argument to a dimer, water molecules are expelled from the space "between" the monomers; hence, on first sight, the number of immobilized solvent molecules would be reduced to N_{tot}(dimer,steric)=2N_{tot}(mono)−2N' where N'≈14 is approximately the number of heavy atoms of a xanthylium moiety. Again, this estimate of N_{tot}(dimer,steric)=60 agrees quite well with the trajectory average of the number of water molecules in the first solvation shell of a P6G dimer, 65.1±4.4. Note that this estimate, alone on steric arguments, would lead to an entropy contribution which would *increase* (in absolute terms) the free energy driving force for dimerization beyond the already very strong energy contribution discussed above.

However, this reasoning solely on steric grounds neglects the long-range electrostatic effect which can be approximately quantified by the electrostatic potential $\Phi \sim q^2/R$ where R is the effective radius of the solute. Upon dimerization, the charge q of the solute doubles, but the effective radius of the solute increases as well, by about a factor of $2^{1/3}$. Therefore, N_{tot}(dimer,steric) has to be scaled by an electrostatic factor:

$$\lambda = \frac{\Phi_{\text{dimer}}}{\Phi_{\text{monomer}}} = \frac{q^2_{\text{dimer}}}{q^2_{\text{monomer}}} \Big/ \frac{R_{\text{dimer}}}{R_{\text{monomer}}} \approx 4/2^{1/3} \sim 3 \qquad (1)$$

Hence, during formation of a dimer, the number of "bound" water molecules is estimated to increase by

$$\begin{aligned} \Delta N &= \lambda N_{\text{tot}}(\text{dimer, steric}) - 2N_{\text{tot}}(\text{mono}) \\ &= (\lambda - 1)2N_{\text{tot}}(\text{mono}) - \lambda 2N' \approx 8N - 6N' \end{aligned} \qquad (2)$$

The estimate for P6G dimerization is ΔN=92. Attributing a change of the free energy by 1 kT due to each of these additionally "bound" solvent molecules, one estimates an entropy induced increase of the free energy upon dimerization by ~55 kcal mol^{-1}. Thus, the total free energy change accompanying the dimerization of P6G is significantly smaller (in absolute terms), about −20 kcal mol^{-1}, than the total energy of dimerization, −77 kcal mol^{-1} (Table 4).

This rather qualitative discussion is corroborated by the results of a free-energy calculation on the dimerization of P6G via thermodynamic integration; see the Section Materials and Methods. The resulting free energy curve (Fig. 8) exhibits a minimum near 3.5–3.8 Å which has a ~7 kcal mol^{-1} depth, in satisfactory agreement with the above estimate.

One expects a rather similar entropy contribution to the free energy change of forming a R6G dimer because the carbethoxyphenyl moieties should hardly affect the number of "bound" water molecules during dimer formation. In

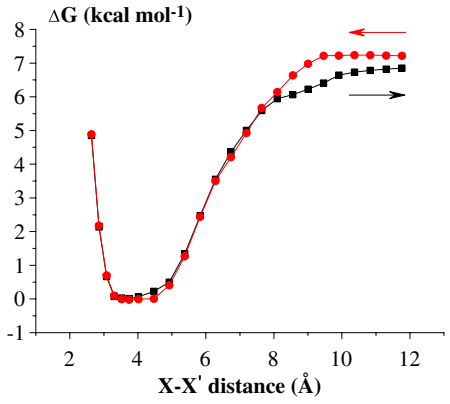

Fig. 8 Free energy profile of a P6G dimer from thermodynamic integration along the centroid distance X–X′ in forward and reverse directions; see also Fig. S2

fact, from the trajectory average of the estimated numbers of water molecules in the first solvation shells of R6G monomers and dimers, 60.1±4.3 and 89.7±5.5, respectively, one deduces that about 30 water molecules are "squeezed" from the first solvation shell upon formation of a R6G dimer, very similar to the trajectory estimate of 25 for the formation of a P6G dimer (see above). Thus, given that dimerization energies of R6G and P6G are similar (Table 4), the free energy change during the formation of an R6G dimer should be similar. However, the solvent induced entropy contribution to the free energy change does not yield an equally satisfactory estimate as for the P6G dimer, in part because of large uncertainty of the dimerization energies (see the relatively large SD values of ~15 kcal mol^{-1}), but most likely because the carbethoxyphenyl substituent of the xanthylium moiety spoils a simple estimate of the Coulomb scaling factor λ. Experimental evidence shows [44–46] that entropy–enthalpy compensation occurs in many chemical and biological processes, resulting in small values of free energies changes.

The driving force of a dimerization reaction often can be expected to be small because the solvent contribution to the dimerization energy scales in very similar fashion as the entropy contribution. We have seen that the total energy of such charged solutes is to a good approximation proportional to the solvation energy, which in turn scales approximately as the electrostatic potential $\Phi \sim q^2/R$. As this latter energy dominates the total energy of dimerization, one has for the energy change during dimerization

$$\begin{aligned} \Delta E_{\text{dim}} &\propto \Phi_{\text{dimer}} - 2 \times \Phi_{\text{monomer}} \\ &\propto -(\lambda - 2)\frac{q^2_{\text{monomer}}}{R_{\text{monomer}}} \sim \Phi_{\text{monomer}} \end{aligned} \qquad (3)$$

Thus, both the energy and the entropy contributions to the dimerization are expected to scale with q^2/R. Inspection of Table 4 shows that the estimate of Eq. 3 holds quite well for P6G and more approximately also for R6G.

Summary and conclusions

In summary, the results of our MD simulations on P6G and R6G dimers do not fully support the computational findings of the work by Daré-Doyen (DD) et al. [7]. We have opted for a different computational protocol. Despite considerable effort, we were not able to reconstruct the DD charge assignment which does not comply with the recommended procedure (referred to as STD) for supplementing the chosen force-field AMBER-95 [16, 25]. Pertinent minima differ by ~10° in the torsion angle for the rotation within the xanthylium dimer. However, we decided to compare for the P6G dimer the results of MD trajectories generated consistently for both charge assignments, STD and DD. In addition, for P6G dimers, we carried out a detailed comparison of an Ewald-type treatment of the Coulomb interaction (PME) with the residue-based cutoff approach chosen previously [7].

Yet, the largest differences by far between the two computational strategies are due to the fact that the previous discussion [7] of the structure of xanthylium dimers was based on too short MD trajectories (1–700 ps) whereas we based interpretation of the structure of dimers on long-time trajectory averages (1,501–2,500 ps). For P6G dimers at long times, averages of structural parameters studied agree well between both force field variants, STD and DD. However, according to our results, the average configuration of a P6G dimer for both set of charges exhibits a "twisted" configuration, closer to a parallel arrangement of the xanthylium groups, in contrast to an anti-parallel configuration assigned previously [7]. Comparison of long-time (1,501–2,500 ps) vs. short-time (1–700 ps) parts of the trajectories exhibits a clear propensity for a further rotation away from the anti-parallel configuration. This confirms that short simulation times [7] are not adequate for sampling the phase space of xanthylium dimers and sheds some doubt on the possibility to compare short-time MD results with NMR data. We found here that the P6G dimer is actually a rather flexible system regarding the torsion angle.

For the R6G dimer, we performed similar investigations, but restricted them to the STD charge assignment and a PME treatment of Coulomb interactions. Starting from an anti-parallel configuration (torsion angle 180°), we observed a trend towards a twisted conformation, with a torsion angle of ~120° along a trajectory of 2.5 ns. In a second trajectory starting with a configuration showing such a torsion angle, we noticed a further torsion toward smaller angles, ~70°. This finding lead us to conclude that even a trajectory of 2.5 ns may not suffice to compare MD findings for R6G dimers with experimental data, in view of the structural complexity introduced by the carbethoxyphenyl substituent of the R6G xanthylium moiety. These aspects require further study.

We also proposed an answer to the question why positively charged xanthylium moieties form dimers (or even higher-order aggregates [4]) in aqueous solution. A quantification of the straightforward argument, which relies on the solvent-induced energy gain as a consequence of the increased charge in the dimer, results in dimerization energies of 60–70 kcal mol^{-1}. This energy is completely dominated by the electrostatic interaction of the solute with its aqueous environment. We showed that a residue-based cutoff strategy and a PME procedure yield compatible values of the electrostatic energy, if a self-interaction correction is applied to PME results of AMBER 8. However, to reach a physically meaningful picture of the dimer formation, one has to turn to a discussion of free energies. For P6G, we proposed an estimate of the solute-solvent entropy change during dimerization, accounting for the reorganization of the solvent in the vicinity of the solute. This entropy related contribution almost cancels the gain in electrostatic energy, as corroborated by a free energy calculation via thermodynamic integration which resulted in driving force for dimerization of only about −7 kcal mol^{-1}. Also these results suggest further studies to arrive at a more complete picture of the structure and dynamics of xanthylium dimers. It will be advantageous to base these investigations on free energy calculations to ensure an unbiased sampling of the phase space.

Acknowledgements We thank M.-E. Michel-Beyerle, E. B. Starikov, A. A. Voityuk, and G. Xiong for helpful discussions. P.C. gratefully acknowledges a Royal Golden Jubilee Scholarship from the Thai Research Foundation and financial support by Deutscher Akademischer Auslandsdienst (DAAD). This work was supported by Volkswagen Foundation, the EU STRP project CIDNA, and Fonds der Chemischen Industrie.

References

1. Selwyn JE, Steinfeld JI (1972) J Phys Chem 76:762–774
2. Wong MM, Schelly ZA (1974) J Phys Chem 78:1891–1895
3. Ilich P, Mishra PK, Macura S, Burghardt TP (1996) Spectrochim Acta A52:1323–1337
4. Toptygin D, Packard BZ, Brand L (1997) Chem Phys Lett 277:430–435
5. Igarashi K, Maeda M, Takao T, Oki Y, Kusama K (1999) Bull Chem Soc Japan 72:1197–1202
6. Ajtai K, Burghardt TP (1995) Biochemistry 34:15943–15952
7. Daré-Doyen S, Doizi D, Guilbaud Ph, Djedaïni-Pilard F, Perly B, Millié Ph (2003) J Phys Chem B 107:13803–13812
8. Penzkofer A, Leupacher W (1987) J Lumin 37:61–72
9. Schimmel PR, Cantor CR (1980) Biophysical Chemistry. Freeman, San Francisco
10. Troxler L, Harrowfield JM, Wipff G (1998) J Phys Chem A 102:6821–6830
11. Wiinja H, Pignatello JJ, Malelani K (2004) J Environ Qual 33:265–275
12. Saenger W (1984) Principles of Nucleic Acid Structure. Springer, Berlin Heidelberg New York
13. Norberg J, Nilsson L (1998) Biophys J 74:394–402
14. Guckian KM, Schweitzer BA, Ren RX-F, Sheils CJ, Tahmassebi DC, Kool ET (2000) J Am Chem Soc 122:2213–2222
15. von Feilitzsch T, Gurzadian GG, Michel-Beyerle ME (2005) private communication
16. Case DA, Darden TA, Cheatham III TE, Simmerling CL, Wang J, Duke RE, Luo R, Merz KM, Wang B, Pearlman DA, Crowley M, Brozell S, Tsui V, Gohlke H, Mongan J, Hornak V, Cui G, Beroza P, Schafmeister C, Caldwell JW, Ross WS, Kollman PA (2004) AMBER 8. University of California, San Francisco

17. Siriwong K, Voityuk AA, Newton MD, Rösch N (2003) J Phys Chem B 107:2595–2601
18. Voityuk AA, Siriwong K, Rösch N (2004) Angew Chem Int Ed 43:624–627
19. Cornell WD, Cieplak P, Bayly CI, Gould IR, Merz KM, Ferguson JDM, Spellmeyr DC, Fox T, Caldwell JW, Kollman PA (1995) J Am Chem Soc 117:5179–5197
20. Wang J, Cieplak P, Kollman PA (2000) J Comp Chem 21:1049–1074
21. Bayly CI, Cieplak P, Cornell WD, Kollman PA (1993) J Phys Chem 97:10269–10280
22. Singh UC, Kollman PA (1984) J Comp Chem 5:129–145
23. Besler BH, Merz KM, Kollman JPA (1990) J Comp Chem 11:431–439
24. Frisch MJ, Trucks GW, Schlegel HB, Scuseria GE, Robb MA, Cheeseman JR, Zakrzewski VG, Montgomery JA, Stratmann RE, Burant JC, Dapprich S, Millam JM, Daniels AD, Kudin KN, Strain MC, Farkas O, Tomasi J, Barone V, Cossi M, Cammi R, Mennucci B, Pomelli C, Adamo C, Clifford S, Ochterski J, Petersson GA, Ayala PY, Cui Q, Morokuma K, Malick DK, Rabuck AD, Raghavachari K, Foresman JB, Cioslowski J, Ortiz JV, Stefanov BB, Liu G, Liashenko A, Piskorz P, Komaromi I, Gomperts R, Martin RL, Fox DJ, Keith T, Al-Laham MA, Peng CY, Nanayakkara A, Gonzalez C, Challacombe M, Gill PMW, Johnson BG, Chen W, Wong MW, Andres JL, Gonzales C, Head-Gordon M, Replogle ES, Pople JA (1998) Gaussian 98. Gaussian Inc, Pittsburgh PA
25. Case DA, Pearlman DA, Caldwell JW, Cheatham III TE, Ross WR, Simmerling CL, Darden TA, Merz KM, Stanton RV, Cheng AL, Vincent JJ, Crowley M, Tsui V, Radmer RJ, Duan Y, Pitera J, Massova I, Seibel GL, Singh UC, Weiner PK, Kollman PA (1999) AMBER 6. University of California, San Francisco
26. Breneman CM, Wiberg KB (1990) J Comp Chem 11:361–373
27. Darden T, York D, Pedersen L (1993) J Chem Phys 98:10089–10092
28. Essmann U, Perera L, Berkowitz ML, Darden T, Lee H, Pedersen LG (1995) J Chem Phys 103:8577–8593
29. Case DA (2005) private communication
30. Jorgensen WL, Chandrasekhar J, Madura JD, Impey RW, Klein ML (1983) J Chem Phys 79:926–935
31. Cheatham III TE, Kollman PA (1996) J Mol Biol 259:434–444
32. Cheatham III TE, Kollman PA (1997) J Am Chem Soc 119:4805–4825
33. Ryckaert J, Cicotti G, Berendsen HJC (1977) J Comput Phys 23:327–335
34. van Gunsteren WF, Berendsen HJC (1977) Mol Phys 34:1311–1327
35. Chipot C, Kollman P, Pearlman D (1996) J Comp Chem 17:1112–1131
36. Tobias DJ, Brooks III CL (1988) J Chem Phys 89:5115–5127
37. Berendsen HJC, Postma JPM, van Gunsteren WF, DiNola A, Haak JR (1984) J Chem Phys 81:3684–3690
38. Hummer G, Pratt LR, Garcia AE (1996) J Phys Chem 100:1206–1215
39. Nijboer BRA, Ruijgrok TW (1988) J Stat Phys 53:361–382
40. Figueirido F, Del Buono GS, Levy RM (1997) J Phys Chem B 101:5622–5623
41. Hummer G, Pratt LR, Garcia AE (1997) J Chem Phys 107:9275–9277
42. Lazaridis T, Paulatis ME (1992) J Phys Chem 96:3847–3855
43. Lazaridis T, Paulatis ME (1994) J Phys Chem 98:635–642
44. Ben-Naim A (1975) Biopolymers 14:1337–1355
45. Kuroki R, Nitta K, Yutani K (1992) J Biol Chem 267:24297–24301
46. Breslauer KJ, Remeta DP, Chou WY, Ferrante R, Curry J, Zaunczkowski D, Snyder JG, Marky LA (1987) Proc Natl Acad Sci USA 84:8922–8926